Experimental Mechanics (2017) 57:675–685
DOI 10.1007/s11340-017-0264-4

The Effect of Grain Size on Deformation and Failure of Ti_2AlC MAX Phase under Thermo-Mechanical Loading

P. Naik Parrikar[1] · **R. Benitez**[2] · **H. Gao**[2] · **M. Radovic**[2,3] · **A. Shukla**[1]

Received: 5 November 2016 / Accepted: 14 February 2017 / Published online: 22 February 2017

Abstract An experimental investigation was performed to analyze the effects of grain size on the quasi-static and dynamic behavior of Ti_2AlC. High-density Ti_2AlC samples of three different grain sizes were densified using Spark Plasma Sintering and Pressureless sintering. A servo-hydraulic testing machine equipped with a vertical split furnace, and SiC pushrods, was used for the quasi-static experiments. Also, a Split Hopkinson Pressure Bar (SHPB) apparatus and an induction coil heating system were used for the dynamic experiments. A series of experiments were conducted at temperatures ranging from 25 °C to 1100 °C for strain rates of 10^{-4} s^{-1} and 400 s^{-1}. The results show that under quasi-static loading the specimens experience a brittle failure for temperatures below Brittle to Plastic Transition Temperature (BPTT) of 900–1000 °C and large deformation at temperatures above the BPTT. During dynamic experiments, the specimens exhibited brittle failure, with the failure transitioning from catastrophic failure at lower temperatures to graceful failure (softening while bearing load) at higher temperatures, and with the propensity for graceful failure increasing with increasing grain size. The compressive strengths of different grain sizes at a given temperature can be related to the grain length by a Hall-Petch type relation.

Keywords MAX phases · SHPB · Hall-Petch effect · Brittle to plastic transition · Kink bands

✉ P. Naik Parrikar
pparrikar@my.uri.edu

[1] Department of Mechanical, Industrial and Systems Engineering, University of Rhode Island, Kingston, RI 02881, USA

[2] Mechanical Engineering Department, Texas A&M University, College Station, TX 77843, USA

[3] Materials Science and Engineering Department, Texas A&M University, College Station, TX 77843, USA

Introduction

Ti_2AlC belongs to a family of ternary carbides and nitrides with hexagonal close packed crystal structure called MAX phases. MAX phases, with the general chemical formula $M_{n+1}AX_n$, are a class of nanolayered, machinable, ternary compounds, where M is an early transition metal, A is a group 13–16 element, X is a carbon and/or nitrogen, and $M_{n+1}X_n$ layers are interleaved with pure A-group element layers [1–3]. MAX phases exhibit a unique combination of properties, including ceramic-like properties such as high-temperature strength, high elastic modulus, and excellent corrosion/oxidation resistance, and metallic-like properties such as good thermal and electrical conductivity, good machinability, thermal shock resistance, and damage tolerance [1–6]. Ti_2AlC has superior oxidation resistance which is attributed to the formation of a well-adhered self-healing Al_2O_3 protective layer [7–12] and has low density (4.11 g/cm3) [3] making it a prospective candidate for some high-temperature applications.

Studies to date on the quasi-static behavior of MAX phases report that mechanical response changes from brittle-like at room temperatures to pseudo-plastic (large deformations with damage accumulation) at elevated temperatures from 900 to 1100 °C [1, 2, 5, 13–15]. MAX phases' stress-strain response in quasi-static cyclic loading is non-linear elastic and hysteretic, with all but the first stress-strain hysteresis loops being closed, reversible and reproducible [16–19]. It is well established by now that dislocation plays an important role in the mechanical behavior of Ti_2AlC and other MAX phases as they are numerous but confined in the basal plane. Basal

plane dislocations can also easily move, multiply, and arrange either in pileups or walls/arrays, even at room temperature. This makes plastic deformation of MAX phases grains highly anisotropic [20–23]. Under applied stress, this plastic anisotropy leads to large internal stresses in the grains unfavorably oriented for deformation by dislocation glide in polycrystalline MAX phase; favorably oriented grains deform easily by basal dislocation glide. In addition to basal plane slip, MAX phase can also deform by kinking, kink band formations, delaminations, microcracks and cavities formations, and grain boundary sliding [1, 2, 5, 24, 25]. Studies have also been conducted to analyze the effect of grain size on the mechanical properties of Ti_3SiC_2 [13, 14, 26] in quasi-static loading conditions. These studies indicate that fine-grained materials exhibit higher compressive strength compared to coarse-grained materials, but at the same time lead to the more brittle and less graceful failure of MAX phases, with smaller hysteresis loops [27].

There have been only a few high strain rate studies [28–30] on MAX phases. Bhattacharya et al. [28] conducted experiments on coarse-grained Ti_2AlC containing many secondary phases (mostly $TiAl_x$ intermetallic) in the 2600–4700 s^{-1} strain rate range, and showed that kinking was an active deformation mechanism, even at high strain rates. Naik Parrikar et al. [30] studied fine-grained Ti_2AlC under quasi-static and dynamic conditions and showed that under dynamic testing conditions, the failure remains predominately brittle even at temperatures as high as 1200 °C. Fracture experiments in that study also revealed that strength and fracture toughness in dynamic conditions are greater than the corresponding quasi-static values by approximately 35% at room temperature and both strength and fracture toughness decrease with increasing temperature. The high temperature and low strain rates were found to promote plastic behavior of fine-grained Ti_2AlC [30]. Most recently, Bhattacharya and Goulbourne [29] characterized strain field evolution in coarse-grained Ti_2AlC during compressive dynamic loading and showed that macro-scale inhomogeneities begin to appear in the strain fields with stresses above 200 MPa; with some regions even experiencing tension. The latter suggests highly non-uniform stress distribution in the Ti_2AlC polycrystalline microstructure in dynamic loading conditions due to the plastic anisotropy of the individual grains.

There is a need to understand the dependence of the mechanical response on grain size under different temperatures and loading rates to better design and develop Ti_2AlC structures. The grain size affects the inhomogeneous stress distribution in the microstructure and different deformation mechanisms such as dislocation glide, kinking, delamination, and grain boundary sliding. The purpose of this study is to address this critical gap in knowledge by investigating the quasi-static and dynamic constitutive behavior of Ti_2AlC with different grain sizes at temperatures ranging from 25 °C to 1100 °C.

Material Fabrication

Description of Sintering Process

A two-step process was used to produce high purity Ti_2AlC for the experiments in this study: Ti_2AlC powders were first synthesized in-house by pressureless sintering, then formed into bulk compact material via Spark Plasma Sintering. Ti (99.5%, −325 mesh), Al (99.5%, −325 mesh) and TiC (99.5%, 2 μm) powders for the synthesis of Ti_2AlC powder were purchased from Alpha Aesar, USA. The powder mixture, with a molar ratio of Ti:Al:TiC =1.00:1.05:0.95, was mixed homogeneously by ball milling for 24 h and then placed in alumina boats and sintered in a high vacuum tube furnace (GSL1600X, MTI Corporation, USA) for 4 h at 1400 °C under Ultra High Purity (UHP) argon flow. After drill-milling and sieving the sintered compact of reacted powder, a 170 mesh Ti_2AlC powder was achieved. It was then densified using Spark Plasma Sintering (SPS)[1] (SPS25–10, Thermal Technology LLC, USA) to produce high-density samples, by sintering for 45 min at 1300 °C. These specimens are referred to as fine-grained, or FG. To create the larger grain size samples while maintaining an invariant amount of impurities, FG samples were further exposed to heat treatment through a high vacuum tube furnace for periods of 8 and 24 h, in UHP argon flow. These samples are designated as medium-grained, MG, and coarse-grained, CG, respectively. Through XRD and SEM analysis, it was found that there was only 3–5% $TiAl_x$ impurity by volume, without any TiC and Ti_3AlC_2 ancillary phases formed.

Micrographs of Grain Sizes

The samples were prepared for microstructural analysis by sectioning on a diamond saw and mounting on a castable mounting material. The samples were then ground and polished with wet SiC abrasive disks from 80 grit SiC to 800 grit followed by fine polishing with polishing cloths and polycrystalline diamond suspensions to 0.1 μm. Etching was performed with a mixture of water, HF and HNO3 1:1:1: for 5 to 20 s to reveal grain boundaries [6]. A back-scattered electron detector was used to obtain the microstructure of the prepared specimens during Scanning Electron Microscopy (SEM). Typical SEM micrographs of the polished and etched surfaces are shown in Fig. 1, illustrating the different grain sizes and morphologies in as-processed samples. The length and thickness of more than 100 grains of each sample were measured using ImageJ (an open source image processing software). The results of the average grain sizes and standard deviation are presented in Table 1. Also, the aspect ratio in

[1] Less common but more appropriately referred to as Electric Current Assisted Sintering (ECAS) or Pulse Eclectic Current Sintering (PECS).

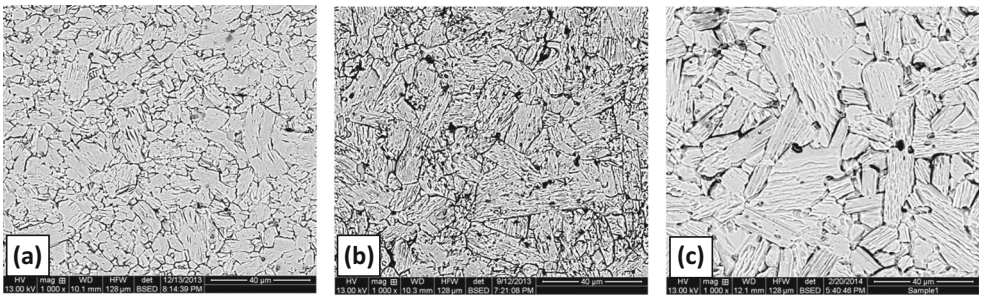

Fig. 1 SEM images of samples with different grain sizes (**a**) FG, (**b**) MG and (**c**) CG

those samples increased monotonically with increasing grain size, as is expected in MAX phases due to their faster growth in the direction of basal planes.

Experimental Setup

Quasi-Static Characterization

Room and high temperature quasi-static uniaxial compression tests were performed using a servohydraulic testing machine (MTS-810, MTS, USA) equipped with a vertical split furnace and SiC pushrods using the procedure detailed in [27]. Cylindrical specimens (5 mm in diameter by 8 mm in length) for the experiments were prepared by wire electron discharge machining (Wire-EDM). Experiments were carried out with fixed crosshead displacement rate to get an initial strain rate of $10^{-4}\ s^{-1}$. A high-temperature axial extensometer (632.59E-77, MTS, USA) was attached to SiC spacers to record displacements, and a K-type thermocouple was placed close to the specimen in direct contact with the spacers to monitor the temperature. Heating rates were limited to less than 600 °C $hr.^{-1}$ and the testing temperature was maintained for 15 min before conducting the experiment. The temperature of the setup was calibrated using a NIST certified calibration thermocouple attached to the sample, and its readings were compared to that of the thermocouple attached to the spacers. The difference in reading after soaking at the target temperature for 15 min was always less than 5 °C. The temperatures provided in this paper are corrected for that difference.

Table 1 Grain sizes of the three samples

Sample	Grain Size		
	Length (μm)	Thickness(μm)	Aspect Ratio
FG	6.1 ± 2.8	4.6 ± 2.2	1.3
MG	13.9 ± 8	7.3 ± 2.4	1.9
CG	17.4 ± 9.7	8.2 ± 2.9	2.1

Dynamic Characterization

Dynamic compression tests at room and high temperature were performed using a modified Split Hopkinson Pressure Bar (SHPB) apparatus (Fig. 2). The striker bar, incident bar and transmission bar in the SHPB setup were all made out of Maraging steel. The incident and transmission bars had a diameter of 12.5 mm and lengths of 2133 mm and 1524 mm, respectively. The Ti_2AlC specimens had a diameter of 5 mm and a thickness of 8 mm. The striker bar was propelled using an air-operated gun. Copper pulse shapers of different thicknesses and diameters were used to control the loading pulse. The pulse shaper was placed at the impact end of the incident bar to generate a linear rising compressive pulse. Two tungsten-carbide (WC) inserts were placed between the two bars and the specimen was sandwiched between the inserts. The impedance of the inserts was matched to that of the bars, so that the inserts did not disturb the stress wave profiles [31–33]. These inserts were used to reduce stress concentration in the specimens and to prevent indentation of the specimens into the bars. Molybdenum disulfide was used to lubricate the specimen-insert interface to minimize the effects of friction. Single pulse loading of the specimen was ensured by using a setup, proposed by Song and Chen [34], that employs a flange attached to the impact end of the incident bar and an associated rigid mass as a momentum trap. A controlled preset gap was maintained between the flange and the rigid mass, that allowed the incident loading pulse to travel but arrested further motion of the incident bar towards the specimen that was caused by the reflected pulse in the incident bar. A Photron SA1 high-speed digital camera was used at a frame rate of 300,000 fps to capture the deformation process. The camera was triggered using an oscilloscope recording strain gage data, resulting in synchronized strain and image measurements.

For high-temperature experiments, an induction coil heater was used with the SHPB setup. Ti_2AlC specimens are electrically conductive and were heated by electromagnetic induction from high current passing through coiled loops around the specimen. The WC inserts prevented the development of a sharp temperature gradient in the bars and also protected the strain gages mounted on the bars. The welding of thermocouples to the specimens was observed to produce minor cracks in them. To avoid this, a calibration procedure was developed wherein a specimen

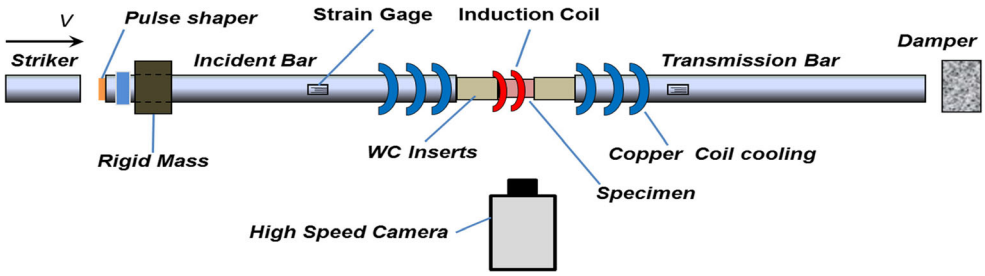

Fig. 2 Schematic representation of SHPB setup

with a thermocouple was used to evaluate the amount of power to be supplied to the induction heating system to achieve the desired steady state temperature in 30–60 s. Fig. 3 shows the temperatures achieved by induction heating in the 1100 °C experiment. The vertical red line indicates the time established to conduct the particular experiment. Several trials were carried out to verify the repeatability of the temperatures achieved and the specimen was found to be within ±15 °C of the target temperature during the trials. This calibrated power was used to heat the specimen during experiments, and the thermocouple was not attached to the specimen directly.

Using one-dimensional wave theory, the strain and stress in the specimen can be determined from the reflected and transmitted strain pulses, respectively, as

$$\sigma_s = E_b \frac{A_b}{A_s} \varepsilon_t(t) \tag{1}$$

$$\varepsilon_s = \frac{-2c_b}{L_s} \int_0^t \varepsilon_r(t)dt \tag{2}$$

Where S_s and e_s are stress and strain in the specimen, ε_r and ε_t are the time resolved strain values of reflected and transmitted pulses, c_b is the longitudinal bar wave speed, E_b is the Young's modulus of the bar material, A_b is the cross-sectional area of the bar, A_s is the cross-sectional area of the specimen, and L_s is the thickness of the specimen. The true stress and true strain were calculated as:

$$\sigma_s = S_s(1-e_s) \tag{3}$$

$$\varepsilon_s = -\ln(1-e_s) \tag{4}$$

The deformations in MAX phases are a combination of plastic deformation and damage accumulation. Equations (3) and (4) are an approximation for MAX phases which help account for increasing cross-sectional area during compression experiments.

Results and Discussion

Quasi-Static Results

Typical stress-strain curves obtained from quasi-static compression testing at different temperatures are shown in Fig. 4. The mechanical response of Ti_2AlC with three different grain sizes is qualitatively similar to the previously reported studies for Ti_2AlC and other MAX phases [35–37] . Below BPTT (~ 900–1000 °C), samples of all grain sizes fail in essentially brittle manner. A very small drop in stress was observed after it reaches maximum value before the catastrophic failure of the specimens. Fine grained samples exhibit higher compressive strengths as compared to other grain sizes. At 900 °C, fine and coarse grained samples showed more graceful failure with a larger softening tail after maximum stress to the point of failure. Above BPTT, at 1000 °C and 1100 °C, all samples deformed pseudo-plastically with large strains to failure exceeding ≈24% and the difference in compressive strengths between samples with different grain sizes getting smaller. Note here that all samples at 1000 and 1100 °C did not fail at strains of 24%, but the tests were stopped as the upper limit of the extensometer was reached at that point. Above the BPTT, the specimens showed some initial softening after reaching maximum stress, that is, stress decreased with increasing strain, and then transition into small apparent hardening with stresses increasing slightly with increasing strain. The transition point from the softening regime to the hardening regime during deformation above BPTT occurs at higher strains with increasing temperature and decreasing grain size. However, this apparent hardening may be an artefact of sample barreling or onset of grain reorientation and grain refinement due to kinking and delamination that might lock the grain boundary sliding.

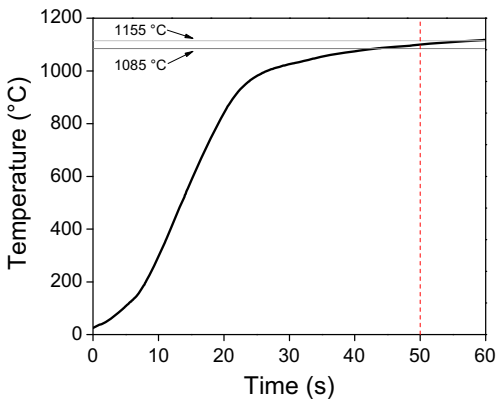

Fig. 3 Evolution of specimen temperature heated using induction heater during an 1100 °C trial

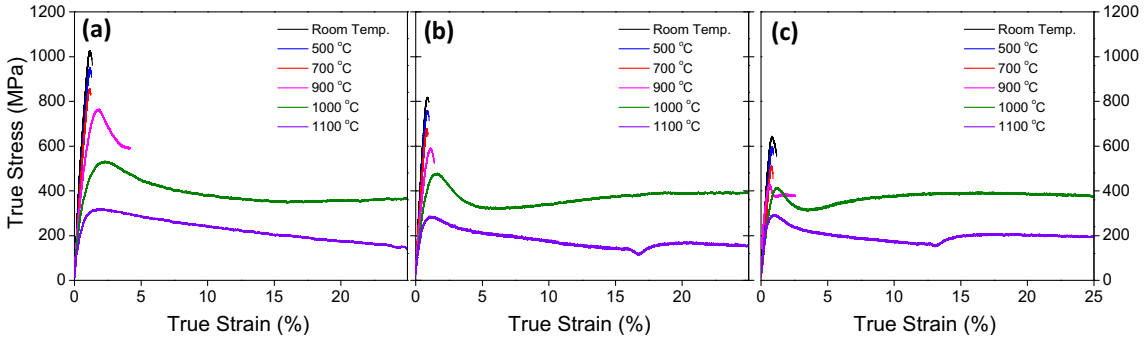

Fig. 4 Quasi-static Stress-Strain curves at different temperatures for (**a**) FG, (**b**) MG and (**c**) CG Ti_2AlC

Dynamic Results

Ti_2AlC specimens displayed catastrophic brittle failure at room temperature and a brittle graceful failure at high temperatures in dynamic loading conditions. Fig. 5(a) illustrates the typical time shifted segments of the recorded pulses while Fig. 5(b) shows the corresponding force ratio variation observed for the specimens which exhibited a catastrophic brittle failure along with the strain evolution with time. As can be seen in Fig. 5(a), the specimen undergoes strain rate acceleration for the first 15 μs causing rising reflected pulse. After 15 μs, and up to the time of failure, the specimen experiences an average strain rate of 400 s^{-1}. The specimen ultimately fails at 38 μs. The occurrence of failure is marked by the peak value of the transmitted pulse, after which the magnitude of transmitted pulse drops sharply. After failure, the magnitude of the reflected pulse rises to the magnitude of the incident pulse. The sharp drop in the transmitted pulse and the rise in the reflected pulse are both characteristic of catastrophic failure. Fig. 5(b) shows that the dynamic stress equilibrium (a force ratio of 1) was attained at about 15 μs and was maintained up to the point of specimen failure. SHPB pulses were analyzed only up to the point of failure (corresponding to peak transmitted pulse) to generate the stress strain curves for the specimens showing catastrophic failure.

Typical pulses, force ratio and strain evolution for a specimen which exhibited a graceful failure are shown Fig. 5(c) and (d). In this case, the transmitted pulse magnitude

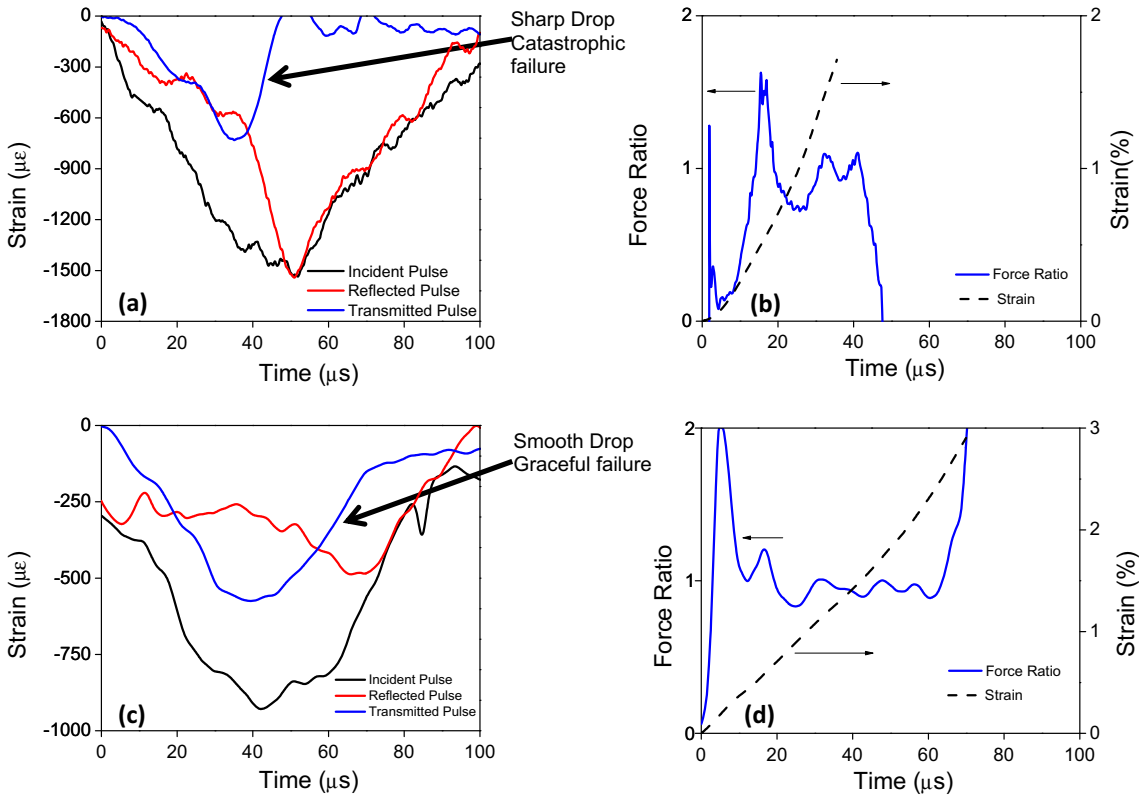

Fig. 5 Recorded pulses illustrating the difference between catastrophic and graceful failure along with force ratio and computed strain corresponding to these pulses

decreases gradually upon reaching its maximum in comparison to the catastrophic failure case. The reflected pulse displays a gradual increase in magnitude signifying an increase in strain rate as the specimen is strained beyond the peak stress state. The strain rate maintained its constant value up to the point of peak stress. The force ratio plot, Fig. 5(d), shows that the specimen is in dynamic equilibrium from 15 μs to 75 μs. The stress-strain curves were generated by analyzing the pulses from the start, up to the point where the specimen was in stress equilibrium.

The true compressive stress-strain curves of fine, medium, and coarse-grained Ti_2AlC during dynamic loading at various temperatures are presented in Fig. 6. Dynamic experiments were conducted at an average nominal strain rate of 400 s^{-1}. The '♦'symbol on the stress-strain curves indicates the point at which equilibrium was established. A '★' symbol is used in these plots to represent points of catastrophic failure. As can be seen in Fig. 6, the peak compressive stress decreases with increase in temperature, similar to what was observed in quasi-static loading; however, that decrease seems to be less significant above BPTT than in quasi-static loading conditions. The specimens had a catastrophic brittle failure at room temperature and a more graceful brittle failure at high temperatures. The temperature at which graceful failure occurs in these specimens decreases with the increase in the grain size. For the dynamic experiments conducted, the graceful failure begins to occur at 1100 °C for fine grain, at 900 °C for medium grain and 600 °C for coarse grain specimens, which is discussed in more detail in the following section.

Compressive Strength

The variation of quasi-static and dynamic compressive strength with temperature and grain size is shown in Fig. 7. For each condition at least three experiments were conducted. Under quasi-static conditions, the compressive strength is a strong function of grain size below BPTT, in both dynamic and quasi static loading conditions. The specimens having smaller grain size had higher compressive strengths, like that in the case of Ti_3SiC_2 [13] . As testing temperature increases above BPTT, compressive strength of fine grained specimens decreases more rapidly and the difference between the compressive strengths of the samples with different grain sizes diminishes, as seen in Fig. 7. This displays good agreement with previous results for MAX phases, namely Ti_3SiC_2, showing that grain size plays a minor role in the mechanical behavior of these materials above BPTT [14].

Dynamic compressive strengths are higher than quasi-static compressive strengths for all grain sizes. This difference between dynamic and quasi-static compressive strength increases with increasing grain sizes below BPTT. Under dynamic conditions, FG specimens displayed greater strength than large grained specimens for all the temperatures investigated. Ti_2AlC displays high compressive strength under dynamic loading at temperatures as high as 1100 °C. Naik Parrikar et al. [30] have also observed such high compressive strengths in Ti_2AlC under dynamic conditions at temperatures up to 1200 °C. Unlike the quasi-static case, decreases in dynamic compressive strength with increasing temperature are relatively linear. This indicates different mechanisms of deformation under quasi-static and dynamic behavior at temperatures above BPTT. This higher strength during dynamic loading is more pronounced at higher temperatures for all grain sizes investigated. Also, although all grain sizes show almost identical compressive strength at 1100 °C in quasi-static conditions, the compressive strengths of the samples with different grain sizes still show a significant difference in dynamic conditions at the same temperature. It has been reported that strain rate sensitivity in MAX phases increases with increasing temperature [13]. Results presented here suggest that at and above BPTT, fine grain structure shows larger strain rate dependence than course grained structures. The latter can be best observed in Fig. 8.

Fig. 8 shows Hall-Petch plot where the average compressive strength at various temperatures for the three grain sizes is plotted as function of $l^{-1/2}$, where l is the average grain length. The linear regression fits have also been shown in the figure. The results indicate Hall-Petch type relationship between the

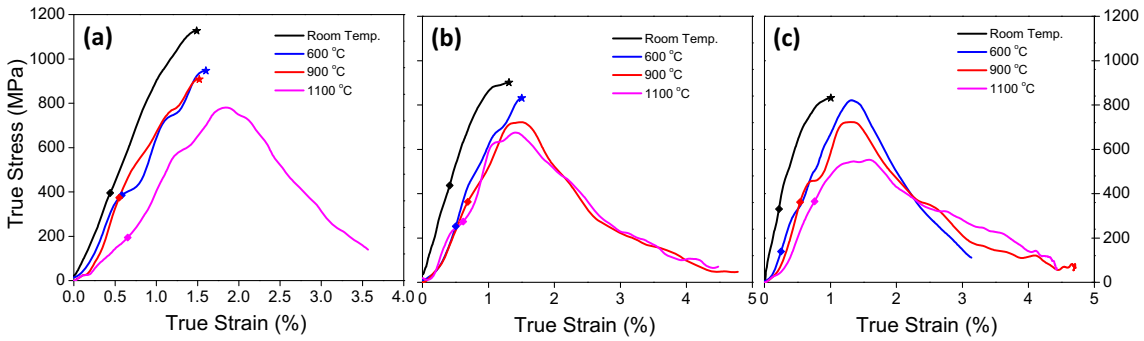

Fig. 6 Dynamic Stress-Strain curves at different temperatures **a** FG, **b** MG and **c** CG

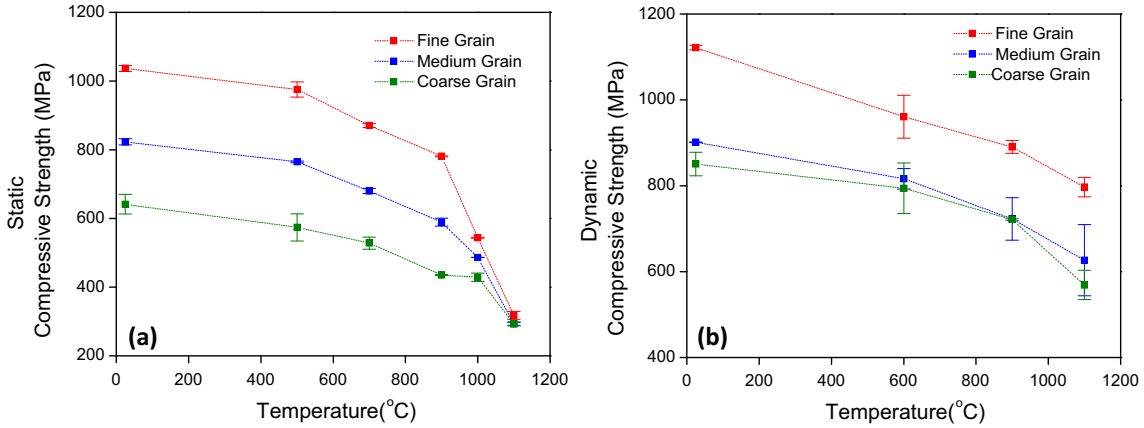

Fig. 7 Compressive strength as a function of grain size and temperature **a** Quasi-static loading and **b** Dynamic loading. The error bars represent the standard deviation from 3 experiments

strength and the grain length under both dynamic and quasi-static loading conditions. The Hall-Petch relation between compressive strength and thickness of grains was also explored, but was found to have low coefficient of determination ($R^2 < 0.6$). The material behavior at the microscale is highly anisotropic. However, as samples for this study were prepared from rapid SPS sintering of randomly distributed powders, no texture is observed in the samples, and their mechanical response can be considered isotropic on macroscale. However, as is typical for MAX phases, the grains in the processed samples are not equiaxial, i.e. they are longer in direction of basal plane and have plate-like shape. This is important because, unlike in ductile materials with more than 5 slip systems, dislocations in MAX phases are limited to basal planes, and therefore good correlation is observed with grain diameter (basal plane length equal to the grain diameter) but not thickness. The Hall-Petch type relationship between strength and grain length can be associated with failure caused by dislocation pile up on grain boundaries between soft and hard grains that in turn leads to high stress concentrations and fracture [27]. In addition, the kinking of hard grains also shows Hall-Petch type dependence with larger grains having higher propensity to buckling and kinking than fine grains. Therefore, below BPTT, strains due to easy slip in the soft grains can be accommodated by buckling, kinking and delamination of the hard grains. Stress concentration due to dislocation pile ups is larger and kinking and delamination is easier in the course grain structure, so the strength of the coarse grain samples is lower than that of the fine grain ones in both quasi static and dynamic conditions. It was also seen that compressive strength decreases more rapidly below BPTT in quasi static than in dynamic loading conditions. This suggests that both piling up of dislocations in soft grains as well as kinking and delamination of hard grains are dynamic processes that depend on loading rate.

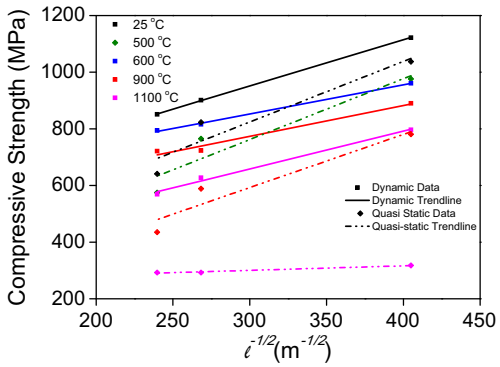

Fig. 8 Hall-Petch relation describing compressive strengths as a function of temperatures for quasi-static and dynamic Loading

For quasi-static loading above BPTT, the slope of the linear fitting line decreases significantly under quasi-static conditions. Even though the mode of dynamic failure is different above BPTT (more graceful), the Hall-Petch relation is still observed. This suggests that the mechanics governing peak compressive strength and the nature of failure (catastrophic or graceful) are different. The peak compressive strength must be driven by the fracture initiation caused by dislocation pile-ups while the catastrophic or graceful failure must be controlled by the crack propagation and the damage containment characteristics of the material. Another possible explanation for this observation is activation of local grain boundary sliding above BPTT to accommodate stress concentrations as was proposed in [2]. Grain boundary sliding is much easier in the fine grain structure, making it more sensitive to loading rate. Stress concentration due to the plastic anisotropy of the individual grains is lower in smaller grains, resulting in higher compressive strengths of FG samples in both quasi-static and dynamic loading conditions below BPTT compared to the CG structure. Stress concentration can be accommodated more easily by grain boundary sliding above BPTT in the FG structure, resulting in a more significant drop of the compressive strength of the FG structure than in the CG structure in a quasi-static loading condition.

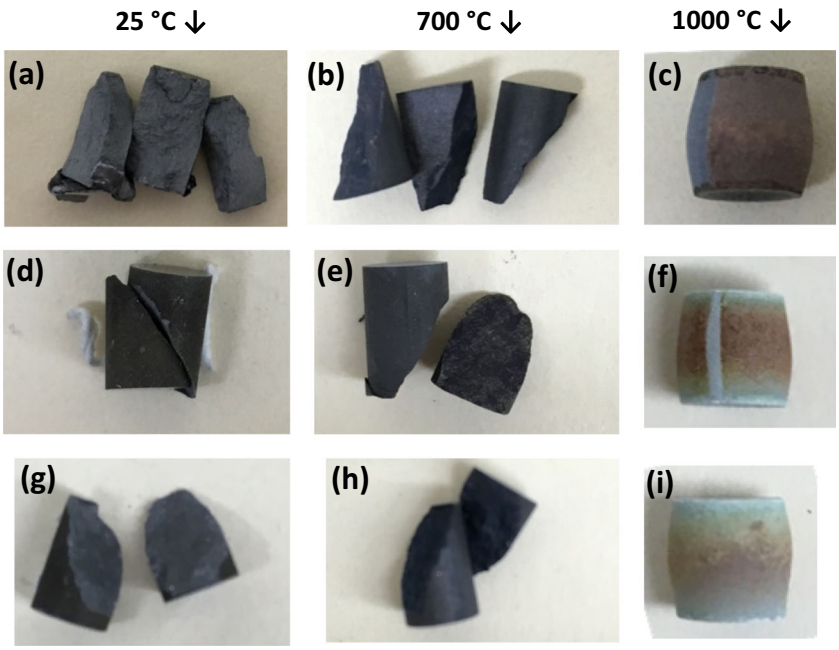

Fig. 9 Post-mortem images of fine grained (**a-c**), medium grained (**d-f**) and coarse grained (**g-i**) specimens after quasi-static loading at 25 °C, 700 °C and 1000 °C

Failure Modes

Post-mortem analysis of the specimens was conducted to study modes of failure. Typical post-mortem images of specimens from quasi-static experiments are shown in Fig. 9. The specimens from quasi-static experiments tested below BPTT fractured with one or two shear cracks. The angle made by the fractured surface with the loading axis varied from 25°- 36°. Above BPTT, specimens did not fail when tested to strains of 24%, and exhibited extensive lateral strains and barreling. Shear failure in MAX phases under compression has been reported in some studies [38–40]. During dynamic experiments, specimens fractured by shear cracks. Post-mortem images of specimens from dynamic experiments are shown in Fig. 10. The high strain rate allows multiple cracks to grow which results in multiple fragments. The difference between catastrophic failure and graceful failure is seen in these images in terms of number of fragments. During a catastrophic failure,

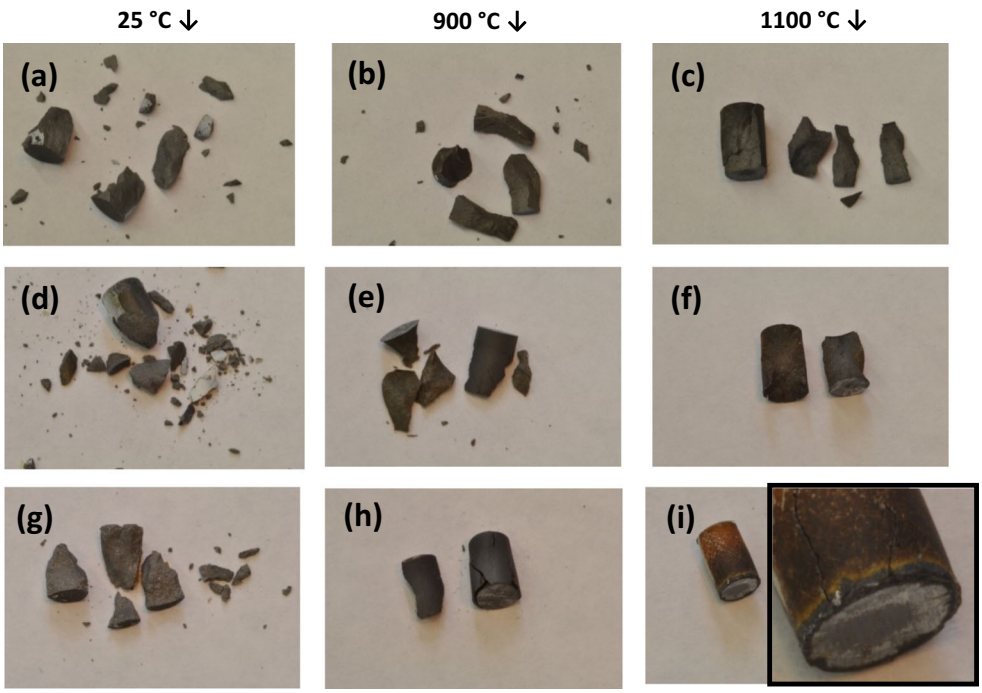

Fig. 10 Post-mortem images of FG (**a-c**), MG (**d-f**) and CG (**g-i**)

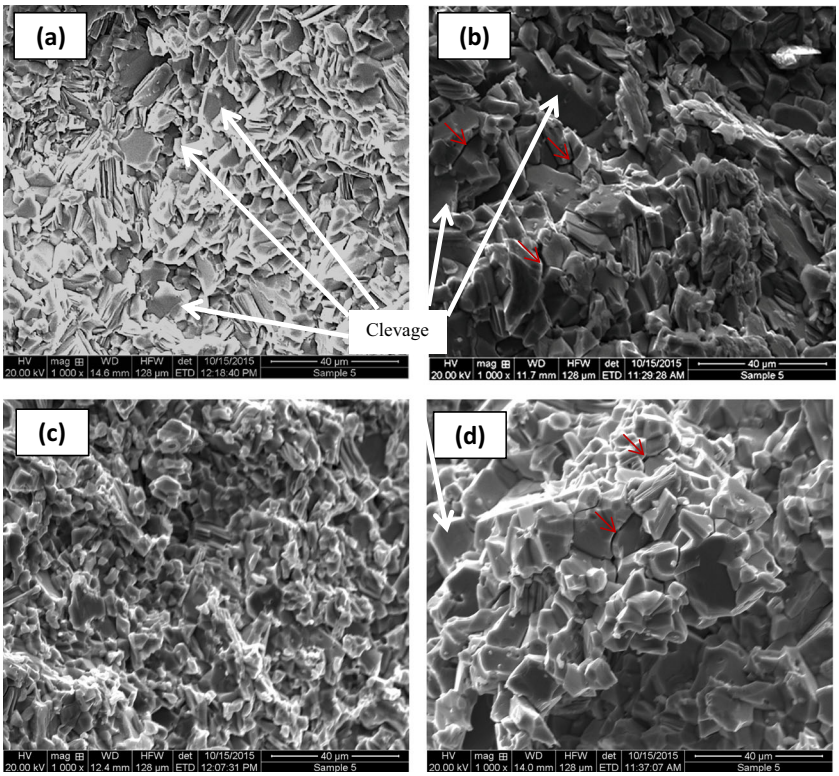

Fig. 11 Fracture surfaces of specimens from dynamic experiments : **a** FG at 22 °C, **b** CG at 22 °C, **c** FG at 1100 °C and **d** CG at 900 °C

a number of small fragments are formed. During graceful failure under dynamic loading, multiple cracks are formed, but the bulk of the specimen stays together. Fig. 10(i) shows a case where coarse-grained Ti_2AlC that was subjected to dynamic load at 1100 °C did not undergo fragmentation, even though there were multiple cracks in the specimen. The difference in the color between samples tested in static and dynamic conditions comes from the different thickness of the oxide layers that forms on the specimens during exposure to high temperature. The oxide layer in static conditions is expected to be thicker. This thickness is only a couple of microns [8, 9] and its effect on the mechanical properties is assumed to be negligible.

Micrographs

Microscopic images of fracture surfaces from the dynamic compression experiments are shown in Fig. 11. Images (a) and (b) depict the specimen fracture surface after dynamic loadings of fine grained and coarse grained specimens at room temperature, respectively. The fracture at room temperature is predominantly intergranular. Images (c) and (d) show fracture surface after dynamic loadings of fine-grained specimens at 1100 °C and coarse-grained specimens at 900 °C, respectively. Coarse-grained specimens at 900 °C were chosen because the specimens at 1100 °C did not fragment. The fracture surfaces have a very rough morphology. The high-temperature

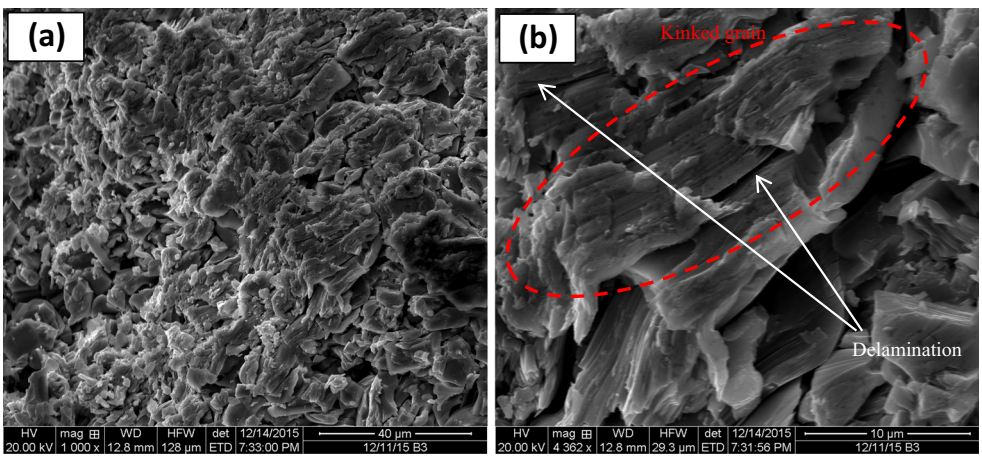

Fig. 12 Fracture surfaces of specimens from dynamic experiments MG at 1100 °C showing **a** grain refinement, and **b** grain kinking and delamination

fracture surfaces show substantial grain refinement. Fig. 12 shows the fracture surface after dynamic loadings of medium grained specimens at 1100 °C at two different magnifications. A combination of cleavage fracture, delamination, and kinking of grains can be observed. The kinking of grains at high temperatures leads to higher energy absorption and enables graceful failure under dynamic loading conditions. Similar observations of kinking being operative under dynamic loading and high temperature, have been reported by Parrikar et al. [30]. Several secondary intergranular cracks (marked as "→") can be seen in the CG microstructure. These secondary cracks facilitate the kinking of grains and might be responsible for the early transition to graceful failure.

Conclusions

An experimental investigation was conducted to evaluate the effect of grain size on the quasi-static and dynamic constitutive behavior of Ti_2AlC. Under quasi-static loading conditions, all three different grain sizes showed brittle failure below 1000 °C (BPTT). At higher temperatures, a brittle to plastic transition was observed. Under dynamic loading conditions, brittle failure was observed for all three gain sizes for all temperatures (up to 1100 °C). A transition from catastrophic failure to graceful failure was observed at higher temperatures, and the propensity of graceful failure increased with increasing grain size. The compressive strengths of different grain size materials were related by a Hall-Petch relation based on grain length. These Hall-Petch relations are valid for temperatures below BPTT for quasi-static loading and valid for temperatures up to 1100 °C for dynamic loading. The results from this study show:

- Compressive strengths measured at dynamic strain rates are higher than strengths measured at quasi-static rates and this difference is more pronounced at higher temperatures.
- The strength of Ti_2AlC is governed by the dislocation pile-up on grain boundaries between soft and hard grains that in turn leads to high-stress concentrations and fracture.
- In quasi-static loading, the compressive strength decreases with increasing grain size till 900 °C. This finding is consistent with the well-known strengthening effects from grain refinement, which is reversed above BPTT due to grain boundary sliding.
- Under dynamic loading, where grain boundary sliding is insignificant, compressive strength decreases with increasing grain size at all temperatures.
- Kinking and delamination of grains during high-temperature dynamic experiments are responsible for the graceful failure.

Acknowledgements The authors would like to acknowledge National Science Foundation funding under Grant No. CMMI 1233887 and CMMI 1233792 at The University of Rhode Island and Texas A&M University. The abstract section has been reproduced from the Ph.D. dissertation of Prathmesh Naik Parrikar (http://digitalcommons.uri.edu/oa_diss/486/).

References

1. Wiley: MAX Phases: Properties of Machinable Ternary Carbides and Nitrides - Michel W. Barsoum. http://www.wiley.com/WileyCDA/WileyTitle/productCd-3527330119.html. Accessed 15 Jun 2015
2. Barsoum MW, Radovic M (2011) Elastic and mechanical properties of the MAX phases. Annu Rev Mater Res 41:195–227. doi:10.1146/annurev-matsci-062910-100448
3. Barsoum MW (2000) The MN + 1AXN phases: a new class of solids: thermodynamically stable nanolaminates. Prog Solid State Chem 28:201–281. doi:10.1016/S0079-6786(00)00006-6
4. Sun ZM (2011) Progress in research and development on MAX phases: a family of layered ternary compounds. Int Mater Rev 56:143–166. doi:10.1179/1743280410Y.0000000001
5. Radovic M, Barsoum MW (2013) MAX phases: bridging the gap between metals and ceramics. Am Ceram Soc Bull 92:20–27
6. Barsoum MW, El-Raghy T (1996) Synthesis and characterization of a remarkable ceramic: Ti3SiC2. J Am Ceram Soc 79:1953–1956. doi:10.1111/j.1151-2916.1996.tb08018.x
7. Yang HJ, Pei YT, Rao JC et al (2011) High temperature healing of Ti2AlC: on the origin of inhomogeneous oxide scale. Scr Mater 65:135–138. doi:10.1016/j.scriptamat.2011.03.031
8. Basu S, Obando N, Gowdy A et al (2011) Long-term oxidation of Ti2AlC in air and water vapor at 1000–1300 °C temperature range. J Electrochem Soc 159:C90–C96. doi:10.1149/2.052202jes
9. Wang XH, Zhou YC (2003) High-temperature oxidation behavior of Ti2AlC in air. Oxid Met 59:303–320. doi:10.1023/A:1023092027697
10. Tallman DJ, Anasori B, Barsoum MW (2013) A critical review of the oxidation of Ti2AlC, Ti3AlC2 and Cr2AlC in air. Math Res Lett 1:115–125. doi:10.1080/21663831.2013.806364
11. Byeon JW, Liu J, Hopkins M et al (2007) Microstructure and residual stress of alumina scale formed on Ti2AlC at high temperature in air. Oxid Met 68:97–111. doi:10.1007/s11085-007-9063-0
12. Sundberg M, Malmqvist G, Magnusson A, El-Raghy T (2004) Alumina forming high temperature silicides and carbides. Ceram Int 30:1899–1904. doi:10.1016/j.ceramint.2003.12.046
13. Radovic M, Barsoum MW, El-Raghy T et al (2002) Effect of temperature, strain rate and grain size on the mechanical response of Ti3SiC2 in tension. Acta Mater 50:1297–1306. doi:10.1016/S1359-6454(01)00424-4
14. Zhen T, Barsoum MW, Kalidindi SR (2005) Effects of temperature, strain rate and grain size on the compressive properties of Ti3SiC2. Acta Mater 53:4163–4171. doi:10.1016/j.actamat.2005.05.020
15. Zhang H, Wang X, Wan P et al (2015) Insights into high-temperature uniaxial compression deformation behavior of Ti3AlC2. J Am Ceram Soc. doi:10.1111/jace.13746
16. Barsoum MW, Zhen T, Kalidindi SR et al (2003) Fully reversible, dislocation-based compressive deformation of Ti3SiC2 to 1 GPa. Nat Mater 2:107–111. doi:10.1038/nmat814
17. Zhou AG, Barsoum MW (2010) Nonlinear elastic deformation of MAX phases. Key Eng Mater 434–435:149–153. doi:10.4028/www.scientific.net/KEM.434-435.149
18. Shamma M, Caspi EN, Anasori B et al (2015) *In situ* neutron diffraction evidence for fully reversible dislocation motion in highly

textured polycrystalline Ti2AlC samples. Acta Mater 98:51–63. doi:10.1016/j.actamat.2015.07.023
19. Benitez R, Kan WH, Gao H et al (2016) Room temperature stress-strain hysteresis in Ti2AlC revisited. Acta Mater 105:294–305. doi:10.1016/j.actamat.2015.12.004
20. Guitton A, Petegem SV, Tromas C et al (2014) Effect of microstructure anisotropy on the deformation of MAX polycrystals studied by in-situ compression combined with neutron diffraction. Appl Phys Lett 104:241910. doi:10.1063/1.4884601
21. Barsoum MW, Farber L, El-Raghy T (1999) Dislocations, kink bands, and room-temperature plasticity of Ti3SiC2. Metall Mater Trans A 30:1727–1738. doi:10.1007/s11661-999-0172-z
22. Farber L (1999) Transmission electron microscopy study of a low-angle boundary in plastically deformed Ti3SiC2. Philos Mag Lett 79:163–170. doi:10.1080/095008399177390
23. Farber L, Barsoum MW, Zavaliangos A et al (1998) Dislocations and stacking faults in Ti3SiC2. J Am Ceram Soc 81:1677–1681. doi:10.1111/j.1151-2916.1998.tb02532.x
24. Barsoum MW, Radovic M (2004) Mechanical properties of the MAX phases. In: Buschow KHJ, Cahn RW, Flemings MC et al (eds) Encyclopedia of materials Science & Technology, 2nd edn. Elsevier, Oxford, pp 1–16
25. Poon B, Ponson L, Zhao J, Ravichandran G (2011) Damage accumulation and hysteretic behavior of MAX phase materials. J Mech Phys Solids 59:2238–2257. doi:10.1016/j.jmps.2011.03.012
26. El-Raghy T, Barsoum MW, Zavaliangos A, Kalidindi SR (1999) Processing and mechanical properties of Ti3SiC2: II, effect of grain size and deformation temperature. J Am Ceram Soc 82:2855–2860. doi:10.1111/j.1151-2916.1999.tb02167.x
27. Benitez R (2015) Effect of microstructure on the mechanical properties of Ti2AlC at room and high temperatures. Thesis
28. Bhattacharya R, Benitez R, Radovic M, Goulbourne NC (2014) High strain-rate response and deformation mechanisms in polycrystalline Ti2AlC. Mater Sci Eng A 598:319–326. doi:10.1016/j.msea.2014.01.032
29. Bhattacharya R, Goulbourne NC (2016) Heterogeneous strain evolution in representative polycrystalline MAX phases. Int J Solids Struct. doi:10.1016/j.ijsolstr.2015.10.002
30. Naik Parrikar P, Benitez R, Gao H et al (2016) Mechanical response of fine grained Ti2AlC under extreme thermo-mechanical loading conditions. Mater Sci Eng A 658:176–184. doi:10.1016/j.msea.2016.01.106
31. Kidane A (2009) An experimental and analytical study of graded materials under thermo-mechanical dynamic loading. Ph.D. Dissertation, National Bible Press
32. Kidane A, Shukla A (2008) Dynamic constitutive behavior of Ti/TiB FGM under thermo-mechanical loading. J Mater Sci 43:2771–2777. doi:10.1007/s10853-008-2520-6
33. Abotula S, Shukla A, Chona R (2011) Dynamic constitutive behavior of Hastelloy X under thermo-mechanical loads. J Mater Sci 46:4971–4979. doi:10.1007/s10853-011-5414-y
34. Song B, Chen W (2004) Loading and unloading split hopkinson pressure bar pulse-shaping techniques for dynamic hysteretic loops. Exp Mech 44:622–627. doi:10.1007/BF02428252
35. Bai Y, He X, Zhu C, Chen G (2012) Microstructures, electrical, thermal, and mechanical properties of bulk Ti2AlC synthesized by self-propagating high-temperature combustion synthesis with pseudo hot isostatic pressing. J Am Ceram Soc 95:358–364. doi:10.1111/j.1551-2916.2011.04934.x
36. Barsoum MW, El-Raghy T, Ali M (2000) Processing and characterization of Ti2AlC, Ti2AlN, and Ti2AlC0. 5 N0. 5. Metall Mater Trans A 31:1857–1865
37. Bai Y, He X, Wang R et al (2013) High temperature physical and mechanical properties of large-scale Ti2AlC bulk synthesized by self-propagating high temperature combustion synthesis with pseudo hot isostatic pressing. J Eur Ceram Soc 33:2435–2445. doi:10.1016/j.jeurceramsoc.2013.04.014
38. Bao YW, Chen JX, Wang XH, Zhou YC (2004) Shear strength and shear failure of layered machinable Ti3AlC2 ceramics. J Eur Ceram Soc 24:855–860. doi:10.1016/S0955-2219(03)00328-5
39. Zhang ZF, Sun ZM (2005) Shear fracture behavior of Ti3SiC2 induced by compression at temperatures below 1000 °C. Mater Sci Eng A 408:64–71. doi:10.1016/j.msea.2005.07.041
40. Bei G-P, Laplanche G, Gauthier-Brunet V et al (2013) Compressive behavior of Ti3AlC2 and Ti3Al0.8Sn0.2C2MAX phases at room temperature. J Am Ceram Soc 96:567–576. doi:10.1111/jace.12092